Neuro-Oncology
25(4), 720–732, 2023 | https://doi.org/10.1093/neuonc/noac261 | Advance Access date 1 December 2022

Inhibition of integrated stress response protects against lipid-induced senescence in hypothalamic neural stem cells in adamantinomatous craniopharyngioma

Chaohu Wang†, Huarong Zhang†, Jun Fan†, Qing Li†, Rongrong Guo†, Jun Pan, Yawei Liu, Junxiang Peng, Qianchao Zhu, Yiwen Feng, Chengdong Wu, Peng Luo, Xiaoyu Qiu, Jin Shi, Yingying Deng, Songtao Qi, and Yi Liu

Department of Neurosurgery, Nanfang Hospital, Southern Medical University, Guangzhou 510515, Guangdong, China (C.Wang, H.Z., J.F, R.G., J.Pan, Y.L., J.Peng, Q.Z., Y.F., C.Wu, P.L., X.Q., J.S., Y.D., S.Q., Y.L.); Department of Dietetics, Nanfang Hospital, Southern Medical University, Guangzhou 510515, Guangdong, China (Q.L.); Central Laboratory, Shunde Hospital, Southern Medical University, Foshan 528300, Guangdong, China (Y.L.)

Corresponding Authors: Songtao Qi, MD, PhD, Department of Neurosurgery, Nanfang Hospital, Southern Medical University, Guangzhou 510515, Guangdong, China (qisongtaonfyy@126.com); Yi Liu, MD, PhD, Department of Neurosurgery, Nanfang Hospital, Southern Medical University, Guangzhou 510515, Guangdong, China (278679433@qq.com).

†These authors are co-first authors and contributed equally.

Abstract

Background. Adamantinomatous craniopharyngioma (ACP) is a benign tumor with malignant clinical manifestations. ACP adjacent to the hypothalamus often presents with more severe symptoms and higher incidence of hypothalamic dysfunction. However, the mechanism underlying hypothalamic dysfunction remains unclear.

Methods. Immunostaining was performed to determine the nerve damage to the floor of the third ventricle (3VF) adjacent to ACP and to examine the recruitment and senescence of hypothalamic neural stem cells (htNSCs). The accumulation of lipid droplets (LDs) in htNSCs was evaluated via BODIPY staining, oil red O staining, and transmission electron microscopy. In vitro and in vivo assays were used to evaluate the effect of cystic fluid or oxidized low-density lipoprotein and that of oxytocin (OXT) on htNSC senescence and the hypothalamic function. The protein expression levels were analyzed using western blotting.

Results. htNSCs with massive LD accumulation were recruited to the damaged 3VF adjacent to ACP. The LDs in htNSCs induced senescence and reduced neuronal differentiation; however, htNSC senescence was effectively prevented by inhibiting either CD36 or integrated stress response (ISR) signaling. Furthermore, OXT pretreatment reduced lipotoxicity via the inhibition of ISR signaling and the repair of the blood–brain barrier.

Conclusions. Reduced LD aggregation or ISR signaling inhibition prevented senescence in htNSCs and identified molecular pathways and potential therapeutic targets that may improve hypothalamic dysfunction in ACP patients.

Key Points

- Nerve injury is prevalent in the 3VF adjacent to ACP.
- htNSCs in a state of lipotoxicity-induced senescence are recruited to damaged 3VF.
- Intervening LD-induced senescence/advance blocking ISR signaling avoids hypothalamic dysfunction.

Adamantinomatous craniopharyngioma (ACP), which is a histologically benign sellar/suprasellar tumor derived from the embryonic remnants of Rathke's pouch, is the most common pituitary tumor in children.[1] ACP is adjacent to the hypothalamic-pituitary axis and other important structures and often causes hypothalamic dysfunction, hypopituitarism, and other complications.[2,3] These complications seriously affect the long-term quality of life of ACP patients[4]; hence,

Graphical Abstract

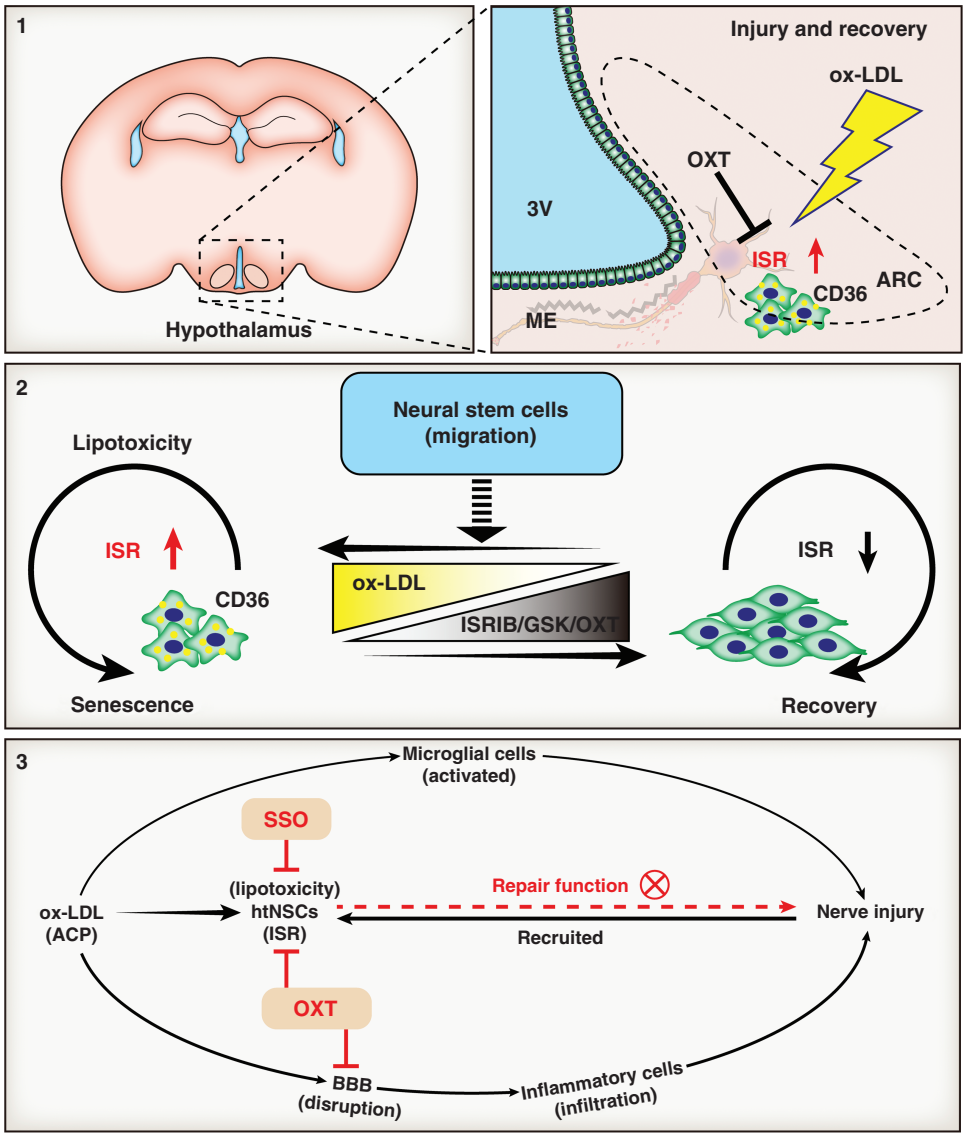

Importance of the Study

Hypothalamic dysfunction due to ACP is common and contributes to the poor quality of life of ACP patients. However, its potential mechanism remains unclear. This study investigated the mechanisms involved in the pathogenesis of hypothalamic nerve damage in ACP patients. Lipid droplets that accumulated in the recruited htNSCs could induce senescence and reduce the neuronal differentiation of htNSCs. htNSC senescence was effectively prevented by inhibiting either the function of scavenger receptor CD36 or the ISR signaling. We elucidated the molecular mechanisms underlying hypothalamic dysfunction and potential therapeutic targets to improve the quality of life of ACP patients.

ACP is considered a pathologically benign and clinically malignant tumor.

Neurological dysfunction is often caused by damage to neurons, axons, the myelin sheath, and other structures.[5] Nevertheless, whether ACP patients with hypothalamic dysfunction experience nerve damage in the hypothalamus has not been reported.

Studies have assessed hypothalamic neural stem cells (htNSCs), which play an important role in nerve injury repair.[6] However, whether htNSCs are involved in the repair of hypothalamic nerve damage, which can improve hypothalamic dysfunction in ACP patients, remains nebulous.

The oily cystic fluid of ACP is rich in lipids. Therefore, ACP is significantly different from other benign tumors of the sellar region.[7] Recently, lipid metabolism disorders triggered by lipid accumulation in adult neural stem/progenitor cells (NSPCs), could lead to the impairment of NSPC proliferation and neurogenesis in the hippocampus.[8]

This was the first study to reveal different degrees of nerve damage in the floor of the third ventricle (3VF) adjacent to ACP, thus resulting in htNSC recruitment to the site of injury. Low-density lipoprotein cholesterol (LDL-C) induced lipotoxicity in the recruited htNSCs, thus leading to senescence and decreased neuronal differentiation. Using transcriptome sequencing analysis, we determined that the integrated stress response (ISR) signaling was the key mechanism involved in htNSC aging. Finally, we demonstrated that oxytocin (OXT) prevented lipotoxicity in htNSCs by blocking ISR signaling and repaired the integrity of the blood–brain barrier (BBB) in the 3VF to limit peripheral inflammatory cell infiltration, thus reducing hypothalamic dysfunction.

Materials and Methods

Detailed materials and methods are provided in Supplementary Materials and Methods.

The Ethics Statements on Human Clinical Samples and Animal Experiments

Clinical samples were collected at the Nanfang Hospital and all patients have signed informed consent to participate in the study according to the ethical protocols of the Ethics Committee of Nanfang Hospital, Southern Medical University. Mice were obtained from the Southern Medical University Animal Center. All animal studies were performed according to the National Institutes of Health *Guide for the Care and Use of Laboratory Animals* and approved by the Experimental Animal Committee of the Nanfang Hospital, Southern Medical University.

Data Availability

The sequencing data are available through NCBI Gene Expression Omnibus (GEO) under the accession number GSE217719.

Results

Nerve Injury is Prevalent in the 3VF Adjacent to ACP

The hypothalamus belongs to the neuroendocrine center (Figure 1A). Preoperative magnetic resonance imaging showed that the 3VF was invaded by ACP with finger-like protrusions (Figure 1B). Furthermore, NF and MBP were only detected in the area away from the tumor, and the structure was relatively intact (Figure 1C). The extent of loss of NF and MBP expression was different among individuals (Figure 1D–G). Surprisingly, the expression of NeuN and MAP2 was almost undetectable in the 3VF adjacent to ACP (Figure 1H). These results indicated that nerve damage in the 3VF adjacent to ACP was widespread, with individual differences. However, only a slight degree of myelin injury occurred in the hypothalamus adjacent to papillary craniopharyngioma (PCP), whereas the structure of neurons in the hypothalamus adjacent to tuberculum sellae meningioma and hypothalamic glioma remained relatively intact (Figure 1F and G, Supplementary Figure 1A–J). Therefore, the hypothalamic nerve injury in the area adjacent to the tumor mainly occurred in ACP.

To further explore the possible reason for hypothalamic nerve injury adjacent to ACP, immunofluorescence staining was performed. The microglia in the damaged area was significantly activated compared with those in the undamaged area (Supplementary Figure 2A and B). Furthermore, microglia were observed to phagocytize myelin debris and hematoxylin and eosin (H&E) staining showed inflammatory cell infiltration around the blood vessel in the 3VF (Supplementary Figure 2C and D). Hence, nerve injury in the hypothalamus may be due to the microglial activation and the destruction of neuronal structures such as axons by infiltrated inflammatory cells (Supplementary Figure 2E). We then established a hypothalamic injury mouse model via the stereotactic microinjection of cystic fluid of ACP to the bilateral ventromedial nucleus of the hypothalamus (VMH) (Supplementary Figure 3A). The microglia were significantly activated, and their number increased and was accompanied by the decrease in the number of neurons in VMH compared with the control and sham groups (Supplementary Figure 3B–F). The treatment of mouse models with BAY 11-7082, an inhibitor of NF-κB signaling, significantly attenuated the number and activation of microglia, and the reduction in the number of VMH neurons was apparently improved compared with that in the cystic fluid group (Supplementary Figure 3B–F). Thus, the microglia in 3VF may be activated by the cystic fluid of ACP and caused the nerve damage in 3VF.

htNSCs are Recruited to the Damaged 3VF Adjacent to ACP

Recently, studies have suggested that adult NSCs are present in the hypothalamus and are involved in systemic aging, reproduction, and damage repair.[6,9] $SOX2^+$ and $Nestin^+$ htNSCs were identified in the 3VF adjacent to ACP

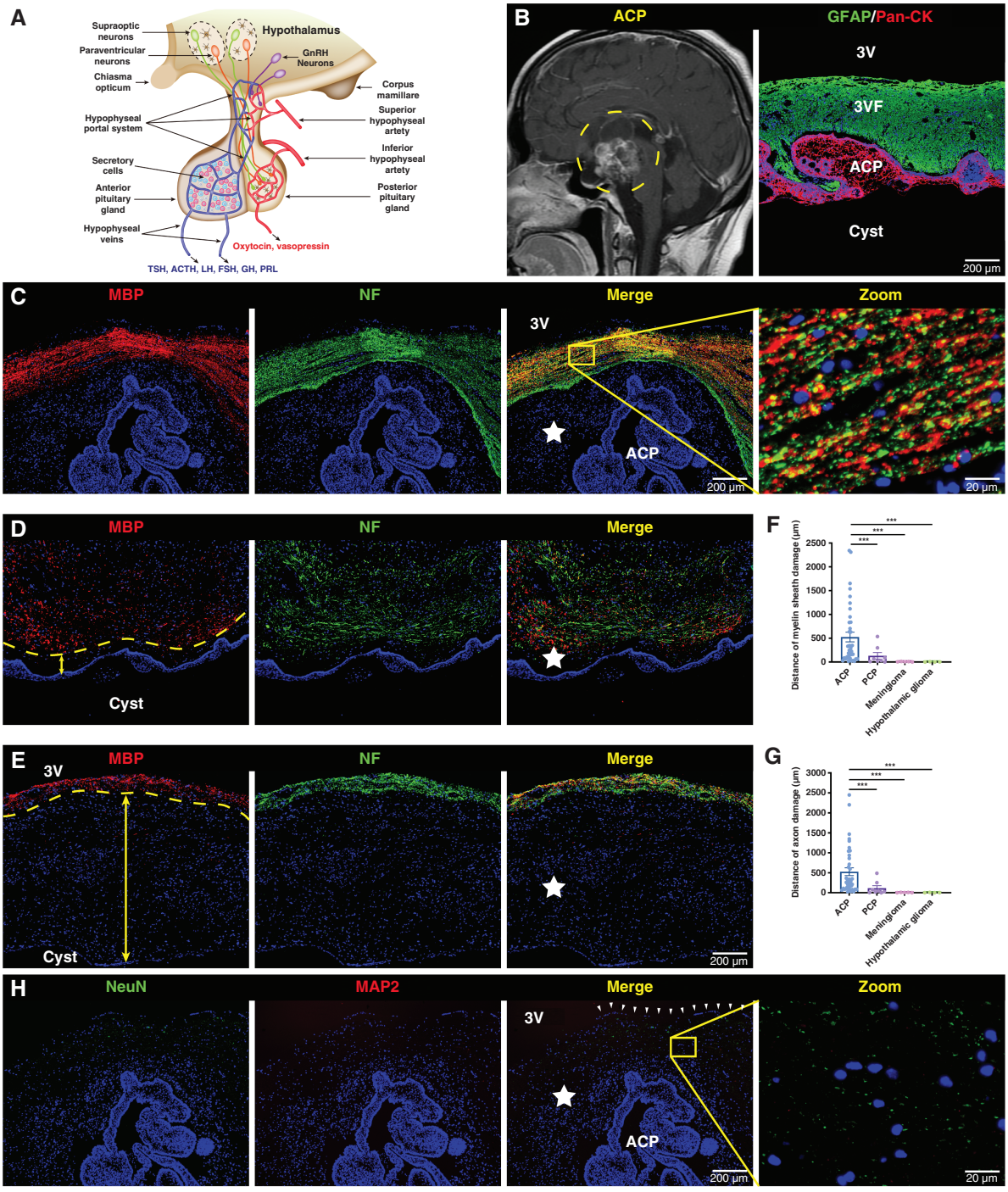

Figure 1. Nerve damage is prevalent in the floor of the third ventricle (3VF) adjacent to adamantinomatous craniopharyngioma (ACP). (A) Representative schematic diagram showing the structures and functions of the hypothalamic-pituitary axis. (B) Representative sagittal contrast-enhanced T1-weighted MR image obtained from a typical ACP patient before surgery (left), and representative immunofluorescence image of pan-cytokeratin (Pan-CK), and glial fibrillary acidic protein (GFAP) staining of ACP tissue samples (right). (C–E) Immunofluorescence staining of ACP tissue samples, representative images of neurofilament (NF), and myelin basic protein (MBP) staining. The five-pointed star represents the damaged 3VF and the arrow represents the damage distance of 3VF. Boxed area is enlarged and presented in right panels. (H) Immunofluorescence staining of ACP tissue samples, representative images of NeuN, and microtubuleassociated protein 2 (MAP2) staining. The arrowheads indicate the ependymal layer of 3VF and the five-pointed star represents the damaged 3VF. Boxed area is enlarged and presented on the right. The cell structure–specific markers used include Pan-CK (ACP tumor cells), NeuN (mature neurons), MAP2 (mature neurons), NF (axons), and MBP (myelin sheath). Data are presented as the mean ± standard error of mean (SEM). $^{*}P < .05$, $^{**}P < .01$, $^{***}P < .001$, NS, not significant. Statistical analysis: (F and G) two-tailed Student's unpaired *t*-test.

(Supplementary Figure 4A and B). These recruited SOX2+ and Nestin+ htNSCs were predominately located in the damaged area that lack NF and MBP expression in the 3VF (Supplementary Figure 4C and D).

Studies have also suggested that htNSCs are mainly distributed in the ependymal layer of the third ventricle wall.[10] We observed that SOX2+ and Nestin+ htNSCs were still visible in the ependymal layer of the 3VF, which was squeezed thin by ACP (Supplementary Figure 5A and B). Tanycyte, as a specialized htNSC, also plays an important role in damage repair.[6] Most htNSCs recruited to the damaged region also expressed tanycyte markers GPR50, Rx, EAAT1, Vimentin, and Connexin 43 (Supplementary Figure 5C–J). Therefore, these htNSCs may recruit from tanycytes with stem cell characteristics in the ependymal layer.

Recruited htNSCs are in a State of DNA Damage and Senescence

Almost no mature neurons were discovered in the 3VF adjacent to ACP (Figure 1I), whereas massive htNSCs were found (Supplementary Figure 4A and B). To explain this paradoxical phenomenon and detect the neuronal differentiation of the recruited htNSCs, we determined that the expression of β3-tubulin and doublecortin (DCX) were negatively expressed in the 3VF adjacent to ACP (Supplementary Figure 6A–D), thus indicating that the recruited htNSCs were not directly differentiated into neurons. Part of these htNSCs expressed oligodendrocyte precursor–related markers SOX9, SOX10, and Olig2 (Supplementary Figure 7A–F); however, mature myelin sheath was still undetectable in the damaged area (Supplementary Figure 7G and H), thus indicating that this subset of htNSCs may constitute oligodendrocyte precursors and have an inhibited function.

The htNSCs were recruited but neuronal differentiation was halted in the damaged 3VF, thus suggesting that htNSCs may not participate in the damage repair of 3VF. Therefore, we hypothesized that the function of these htNSCs was suppressed. We found that Ki-67 and MCM2 were only expressed in few htNSCs (Figure 2A and B, Supplementary Figure 8A and B). We then evaluated the expression of DNA damage marker γ-H2AX and senescence markers Lamin B1, H3K9Me3, P21, and P16 in the recruited htNSCs. γ-H2AX and P21 were highly expressed in most recruited htNSCs, whereas Lamin B1 and H3K9Me3 expressions were downregulated in the β-catenin-accumulating clusters and the majority of htNSCs (Figure 2C–F, Supplementary Figure 8C–E, I). Another senescence marker, P16, was mainly expressed in ACP cells, particularly in β-catenin-accumulating clusters, and only a small number of htNSCs was positive for P16 (Supplementary Figure 8F–H, J).

Therefore, the recruited htNSCs suffered from DNA damage and senescence, thus significantly inhibiting proliferation and neuronal differentiation.

Lipid Droplet (LD) Accumulation is Toxic to the Recruited htNSCs

ACP was predominantly solid cystic. The cysts were rich in cholesterol, which caused severe adhesion and massive cholesterol clefts in the 3VF tissue (Figure 3A–D). The LDL-C concentration in the cystic fluid of ACP was significantly higher than that in PCP, with significant individual differences (Supplementary Figure 9A). We then assessed the presence of lipid deposition in the 3VF tissue adjacent to ACP. Compared with normal brain (NB) tissue, Filipin, Oil red O (ORO) and BODIPY staining revealed a higher content of LDs in the 3VF adjacent to ACP (Figure 3E–G). We preliminarily explored the possible source of lipids in the cystic fluid. First, H&E, Filipin and ORO staining revealed massive LDs in the cysts of ACP and the ACP tissue around the cysts (Supplementary Figure 9B–E). Secondly, transcriptome sequencing and bioinformatics analysis were applied, and the results of gene set enrichment analysis (GSEA) showed that, compared with PCP and nonfunctional pituitary adenoma (NFPA), the pathways related to cholesterol biosynthesis, cholesterol efflux, and triglyceride metabolism were significantly upregulated in ACP (Supplementary Figure 10A–D). Subsequently, quantitative real-time polymerase chain reaction (qRT-PCR) assay showed that ACP expressed a much higher level of cholesterol biosynthesis-associated genes, namely, *SREBF2*, *SREBF1*, and *HMGCR*, and cholesterol efflux-associated gene *ABCA1* than PCP and NFPA (Supplementary Figure 10E). The expression of cholesterol efflux key protein liver X receptor α (LXRα) was closely associated with the β-catenin-accumulating clusters (Supplementary Figure 10F). Gene interaction network analysis also indicated that *CTNNB1* (β-catenin encoding gene) strongly interacted with *NR1H3* (LXRα encoding gene) (Supplementary Figure 10G). These results suggest that ACP was in an aberrant metabolic state of high synthesis and high efflux cholesterol, and high lipid concentration was accumulated in both the cystic fluid of ACP and adjacent 3VF tissue.

To determine whether the LDs from ACP aggregated in the recruited htNSCs, we used magnetic-activated cell sorting to purify the htNSCs adjacent to ACP and the relatively normal NSCs of the subventricular zone (SVZ) away from the frontal glioma (Figure 3H and I) and analyzed these NSCs by using transmission electron microscopy. The results demonstrated that htNSCs contained a larger number of LDs than the NSCs of SVZ (Figure 3J). Meanwhile, the content of TAGs and total FAs in htNSCs were significantly higher than those of NSCs of SVZ (Figure 3K and L), indicating that htNSCs may suffer from lipotoxicity following LD aggregation and may result in DNA damage and senescence.

The entry of exogenous LDL-C into cells is mediated by the receptors on the cell membrane, including CD36, LDLR, MSR1, SCARB1, and OLR1.[11] Compared with the NSCs of SVZ, the mRNA expression levels of *CD36* and *SCARB1* were upregulated in htNSCs, among which CD36 was more significantly upregulated (Supplementary Figure 11A). Immunofluorescence staining showed that CD36 was mainly co-localized with Nestin+ htNSCs, but with few microglia (Supplementary Figure 11B–E). These results suggest that LDs may aggregated in htNSCs via CD36.

To verify that LDL-C was responsible for the lipotoxicity of htNSCs adjacent to ACP, we analyzed mouse hypothalamus-derived htNSCs with different ways of stimulating (Supplementary Figures 12 and 13). The htNSCs were stimulated by the cystic fluid or oxidized low-density

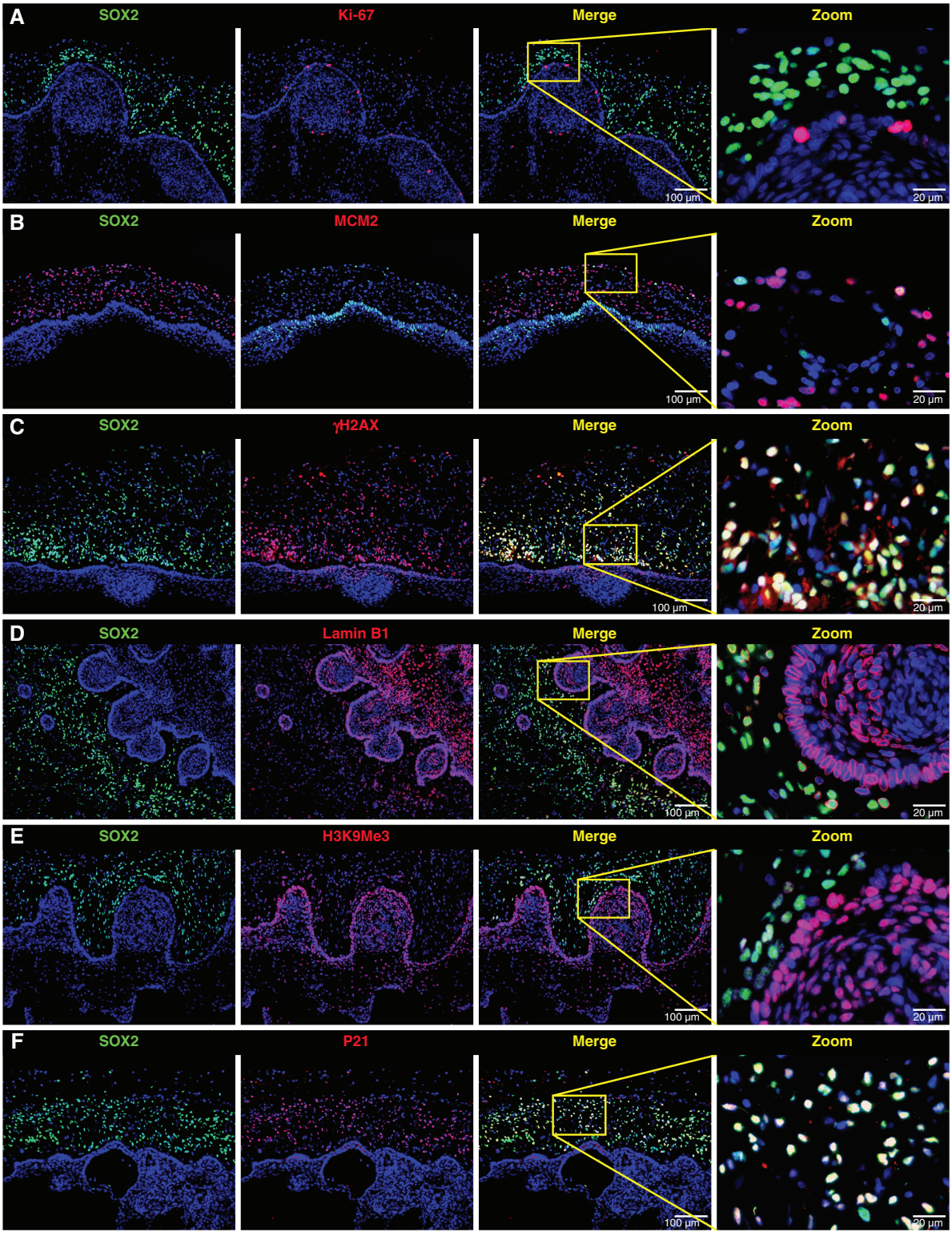

Figure 2. Recruited hypothalamic neural stem cells are in a state of DNA damage and senescence. (A–F) Double immunofluorescence staining of ACP tissue samples; representative images showing the co-expression of SOX2 and different markers (Ki-67, MCM2, γ-H2AX, Lamin B1, H3K9Me3, P21). Ki-67 and MCM2 are both proliferative-specific markers; γ-H2AX is a DNA damage-specific marker; senescence-specific markers used are Lamin B1, H3K9Me3, and P21. Boxed area is enlarged and presented on the right.

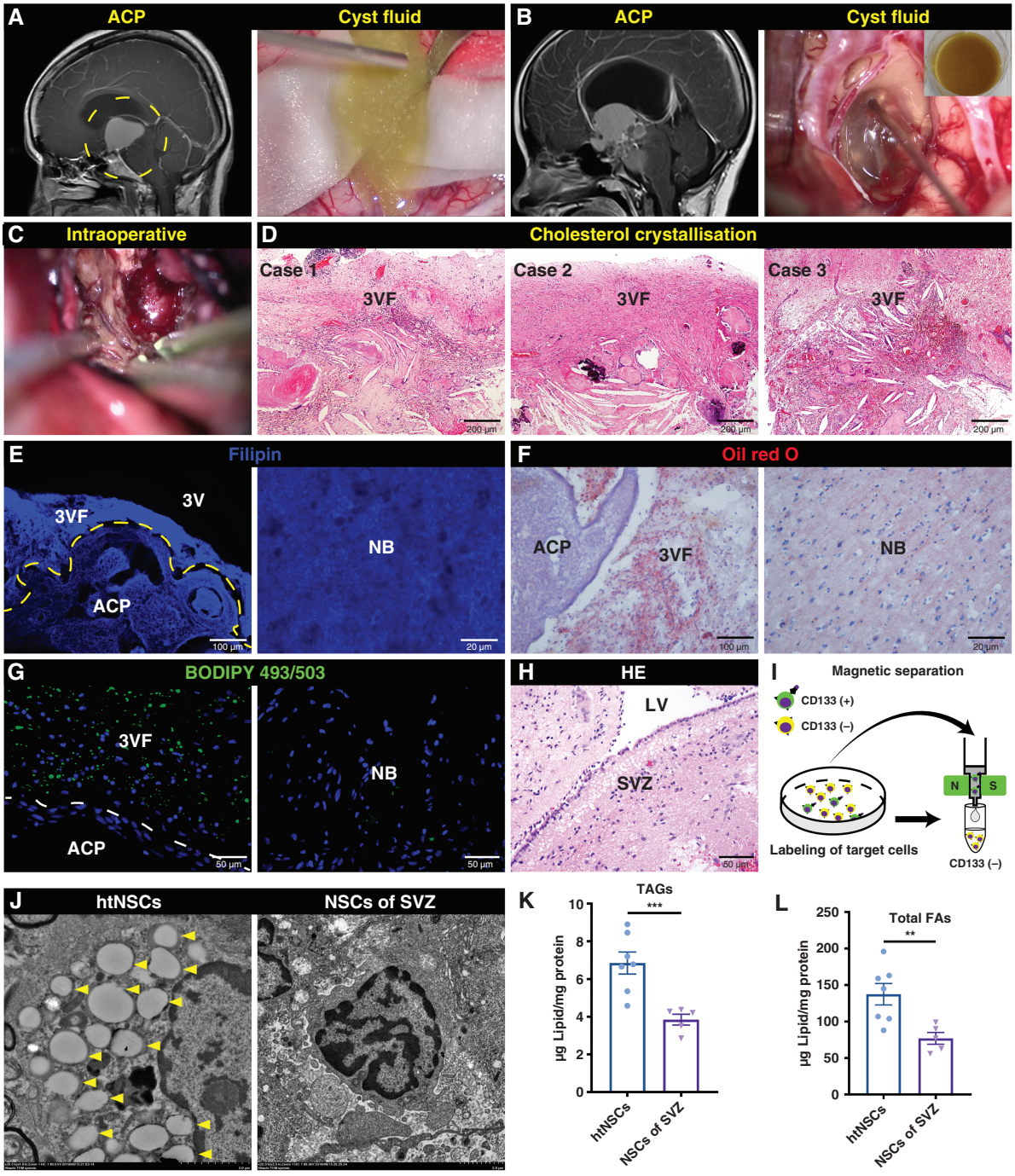

Figure 3. Lipid droplets are aggregated in the recruited htNSCs. (A–C) Representative sagittal contrast-enhanced T1-weighted MR images (left of A and B) obtained before surgery and representative intraoperative images (right of A and B; C) of two typical cystic ACP patients. (D) Hematoxylin and eosin (H&E) staining of three ACP tissue sections; representative images showing the cholesterol clefts in the 3VF adjacent to ACP. (E–G) Filipin staining (E), oil red O (ORO) staining (F), and BODIPY staining (G) of the 3VF adjacent to ACP and NB; representative images are shown. (H) H&E staining of the subventricular zone (SVZ) from NB; representative images are shown. (I) Schematic diagram showing magnetic-activated cell sorting of NSCs using CD133 microbeads. (J) Representative transmission electron microscopy micrographs of LDs in CD133+ NSCs obtained from the 3VF adjacent to ACP or SVZ of NB. The arrowheads indicate the LDs in NSCs. (K and L) Quantification of triacylglycerols (TAGs; K) and total fatty acids (FAs; L) levels in $CD133^+$ NSCs obtained from the 3VF adjacent to ACP ($n = 7$) and SVZ of NB ($n = 5$); in vitro measurement. Data are presented as the mean ± SEM. $^*P < .05$, $^{**}P < .01$, $^{***}P < .001$, NS, not significant. Statistical analysis: (K) two-tailed Student's unpaired *t*-test. LV, lateral ventricle.

lipoprotein (ox-LDL) for 72 h. The percentage of senescent cells (senescence-associated β-galactosidase, SA-β-Gal+) was significantly higher than that of the control group; however, the percentage of senescent cells in htNSCs pretreated with CD36 inhibitor sulfo-N-succinimidyl oleate (SSO) for 12 h did not increase notably (Supplementary Figure 14A and B). Similarly, the neurospheres pretreated with SSO were not affected by ox-LDL (Supplementary Figure 14C–E). In vitro neuronal differentiation analysis showed that htNSCs pretreated with SSO were not affected by ox-LDL (Supplementary Figure 14F and G). This inhibitory effect was similar to the results of the histopathological analysis (Supplementary Figure 6B and C). Finally, htNSCs treated with cystic fluid or ox-LDL had significantly higher p21 Waf1/Cip1 and γ-H2AX protein levels and significantly lower Cyclin D1 and PCNA protein levels than those in the control group. However, pretreatment with SSO blocked these effects (Supplementary Figure 14H); which was consistent with SA-β-Gal staining and in vitro neurosphere assays.

To investigate the underlying mechanism of SSO in blocking the effect of ox-LDL on htNSCs, we discovered LD aggregation increased in htNSCs treated with cystic fluid or ox-LDL compared with that in the control group; however, no significant LD aggregation was observed in htNSCs pretreated with SSO (Supplementary Figure 15A–D). The excessive accumulation of LD in cells induces lipid peroxidation and mitochondrial damage, thus resulting in cellular dysfunction. To assess lipid peroxidation, we used BODIPY 581/591 C11 (BD-C11) ratiometric lipid peroxidation sensor. The BD-C11 ratio (green to red) increased in htNSCs treated with cystic fluid or ox-LDL, thus indicating higher levels of lipid peroxidation. By contrast, pretreatment with SSO blocked this effect (Supplementary Figure 16A and B). Subsequently, we discovered the mitochondria were damaged by excessive LD accumulation; however, SSO pretreatment largely blocked these effects (Supplementary Figure 17A–C). Cystic fluid or ox-LDL might have accumulated in the htNSCs via CD36, thus resulting in lipid peroxidation, mitochondrial damage, senescence, and subsequent functional impairment of htNSCs, whereas SSO effectively blocked this damage effect.

RNA Sequencing Analysis Reveals that ISR Signaling is Activated in Lipotoxic htNSCs

Loss of protein homeostasis is associated with various age-related diseases.[12,13] ISR signaling is a cellular signaling network induced by extracellular stress and is responsible for the maintenance of cellular homeostasis by, for example, controlling protein synthesis rate.[14] To determine whether ISR signaling participates in inhibiting htNSC function due to cystic fluid or ox-LDL, we used an unbiased RNA sequencing (RNA-seq) transcriptome profiling approach to compare htNSCs from 3VF adjacent to ACP and NSCs from SVZ (Supplementary Figure 18A, Figure 3H and I). Owing to the high expression of CD133 in β-catenin-accumulating clusters of ACP, we first excluded the interference from β-catenin-accumulating clusters. The GSEA indicated that the pathways were significantly enriched in β-catenin-accumulating clusters in previous studies, including the FGF, SHH, and WNT pathways were not significantly enriched in htNSCs, except for the BMP pathway (Supplementary Figure 18B). Senescence-associated secretory phenotype (SASP) was significantly enriched in htNSCs (Supplementary Figure 18C). SASP-targeted genes, including *CDKN1A*, *CDKN2A*, *IL-1B*, *IL-8*, *IL-6*, *CCL-2*, and *VEGFA*, were also significantly increased in htNSCs (Supplementary Figure 18D). Positive SA-β-Gal staining, along with the decreased expression of Lamin B1 and H3K9Me3 in htNSCs, confirmed the senescence phenotype of htNSCs (Supplementary Figure 18E–J).

Principal component analysis and hierarchical clustering showed a significant difference between the htNSCs and NSCs of SVZ (Supplementary Figure 19A and B). Analysis of differentially expressed genes (DEGs) between the two groups determined a total of 1055 DEGs. Compared with NSCs of SVZ, 501 genes were upregulated in htNSCs, and 554 were downregulated; the expression of ISR-related genes, including *ATF4*, *EIF2AK3*, *EIF2AK4*, and *DDIT3*, was significantly upregulated in htNSCs. Senescence-associated gene *CDKN1A*, DNA damage-related gene *H2AFX*, and LDL-C receptor-related gene *CD36* were also dramatically upregulated in htNSCs (Supplementary Figure 19C, Supplementary Table 7). We performed GSEA and determined that genes related to ISR signaling were enriched in htNSCs (Supplementary Figure 19D). We validated the expression of ISR-related genes, such as *ATF4*, *EIF2AK4*, and *DDIT3*, by using qRT-PCR, and confirmed the RNA-seq results (Supplementary Figure 19E). These results suggest that ISR signaling was upregulated in htNSCs and may play an important role in the htNSC senescence induced by ox-LDL.

Inhibition of ISR Signaling Blocks Lipid-Induced Senescence in htNSCs

The ISR signaling in htNSCs could be activated by cystic fluid or ox-LDL for 72 h, however, the pretreatment of htNSCs with selective PERK inhibitor GSK2606414 (GSK) at 2 μM or eIF-2α inhibitor ISRIB at 200 nM for 2 h blocked the ox-LDL-induced upregulation of phospho-eIF-2α, ATF4, and CHOP (Supplementary Figure 19F). Furthermore, the pretreatment of htNSCs with GSK or ISRIB inhibited the upregulation of p21 Waf1/Cip1 and γ-H2AX and the downregulation of Cyclin D1 and PCNA induced by ox-LDL (Supplementary Figure 19G). Therefore, ISR signaling was activated by cystic fluid or ox-LDL in htNSCs and could be blocked by GSK or ISRIB pretreatment.

We evaluated the effect of ISR inhibition on the senescence and dysfunction of htNSCs induced by cystic fluid or ox-LDL. The in vitro cell senescence assays indicated that ox-LDL-induced senescence parameters in htNSCs were significantly reduced by GSK or ISRIB pretreatment (Supplementary Figures 19H and 20A). The in vitro neurosphere assay showed that GSK or ISRIB pretreatment also attenuated the effects of ox-LDL in reducing the number and size of hypothalamic neurospheres (Supplementary Figures 19I, J and 20B). Furthermore, the decrease of the neuronal differentiation of htNSCs induced by ox-LDL was inhibited by pretreatment with GSK or ISRIB (Supplementary Figures 19K and 20C). BODIPY staining

showed that the number of LDs in htNSCs pretreated with GSK or ISRIB was comparable with that of htNSCs treated with cystic fluid or ox-LDL (Supplementary Figure 21A and B). These results suggest that ISR signaling blockade inhibited the senescence and dysfunction of htNSCs induced by cystic fluid or ox-LDL; however, the entrance of ox-LDL into htNSCs was not prevented by ISR signaling blockade.

Recent studies have reported that the hypothalamic dysfunction was significantly improved following intranasal OXT supplementation.[15,16] Moreover, OXT not only suppressed SASP-induced senescence in normal human dermal fibroblasts (NHDFs) by OXT receptor (OXTR)–mediated extracellular signal–regulated kinase/Nrf2 signaling[17] but also suppressed inflammatory responses induced by lipopolysaccharide (LPS) via the inhibition of the eIF-2α-ATF4 pathway in mouse microglia.[18] In our previous work, OXTR was co-expressed in htNSCs, and the axons transporting OXT were damaged in 3VF adjacent to ACP (Supplementary Figure 22A and B). Therefore, we investigated whether OXT could prevent htNSC senescence by inhibiting ISR signaling; OXT treatment attenuated the effects of ox-LDL by increasing the protein levels of phospho-eIF-2α, ATF4, CHOP, p21 Waf1/Cip1, and γ-H2AX and by decreasing the protein levels of Cyclin D1 and PCNA; furthermore, OXTR antagonist (OTRA) L-371,257 significantly reversed the suppressive effects of OXT (Supplementary Figure 22C and D).

To further verify the cytotoxic effects of cystic fluid and ox-LDL in vivo, we injected cystic fluid or ox-LDL into one side of the lateral ventricle of mice, whereas the other side was injected with inhibitors (SSO, ISRIB, GSK) or OXT (Supplementary Figure 22E). BODIPY staining showed that, compared with the control and sham groups, a large number of LD accumulated in the ependymal cells of the third ventricle (3V), whereas pretreatment with SSO for 1 week significantly reduced the accumulation of LDs (Supplementary Figure 22F and G). The inhibition of ISR signaling with one-week OXT, GSK, or ISRIB pretreatment had no significant effect on the aggregation of LDs in the ependymal cells induced by cystic fluid or ox-LDL in vivo (Supplementary Figure 22F and G); this was consistent with our in vitro results. Subsequently, we performed qRT-PCR; the mRNA expression levels of ISR-related genes *ATF4* and *DDIT3* and senescence-related gene *CDKN1A* were significantly upregulated in the arcuate nucleus (ARC) and median eminence (ME) after stimulation with cystic fluid or ox-LDL compared with the control and sham groups; the upregulation of these ox-LDL-induced genes was blocked by SSO, GSK, ISRIB, or OXT pretreatment (Supplementary Figure 22H, I and K). However, the mRNA expression level of DNA damage-related gene *H2AFX* was only upregulated in ACP cystic fluid group, while no significant difference was found in other groups (Supplementary Figure 22J).

These results indicate that cystic fluid or ox-LDL induced lipotoxicity in htNSCs both in vivo and in vitro. SSO improved the function of htNSCs by blocking the entry of ox-LDL into htNSCs and preventing the activation of ISR signaling. Although ISR inhibitors and OXT could not block ox-LDL from entering htNSCs, they prevented htNSC senescence by inhibiting ISR downstream signaling (Supplementary Figure 22L).

OXT Repairs the Damaged BBB and Ameliorates Hypothalamic Dysfunction and Cognitive Decline In Vivo

Interestingly, we observed IBA1$^+$ and CD169$^+$ peripheral mononuclear macrophages and CD3$^+$ lymphocytes were infiltrated in the 3VF adjacent to ACP (Supplementary Figure 23A and B). Simultaneously, the expression of ZO-1 was downregulated in the vascular walls of 3VF and the ependymal layer of 3V, thus resulting in plasma albumin diffused into the 3VF (Supplementary Figure 23C). These results confirmed the impairment of BBB in the 3VF adjacent to ACP, thus suggesting that lipids from peripheral blood may enter the 3VF, further aggravating the lipotoxicity in htNSCs. The OXTR was highly expressed in the vascular walls of the 3VF adjacent to ACP (Supplementary Figure 23D). Therefore, OXT may participate in the repair of damaged BBB in the 3VF and prevent lipotoxicity in htNSCs.

To test our hypothesis in vivo, we performed immunofluorescence staining in the mouse models described above and showed that, compared with the control and sham groups, the expression of Lamin B1 and H3K9Me3 were decreased in the SOX2$^+$ NSCs of ME and the ependymal layer of mice treated with cystic fluid or ox-LDL; however, mice pretreated with OXT for one week remarkably prevented the downregulation of Lamin B1 and H3K9Me3 induced by ox-LDL in SOX2$^+$ NSCs (Supplementary Figure 24A, B, E and F). ZO-1 expression was significantly decreased in the ependymal layer of the 3V and the vascular walls of ARC compared with the control and sham groups; however, 1-week pretreatment with OXT significantly reduced the BBB destruction induced by ox-LDL (Supplementary Figure 24C and G). We also observed significant CD169$^+$ peripheral mononuclear macrophage infiltration, which was significantly inhibited by one-week of OXT pretreatment (Supplementary Figure 24D and H). The above effects of OXT was blocked by OTRA pretreatment (Supplementary Figure 24I–L), thus suggesting that OXT acts via OXTR. OXT not only prevented the dysfunction of htNSCs by blocking ISR signaling but also reduced peripheral immune cell infiltration by repairing the damaged BBB in the 3VF; this confirms our hypothesis.

Compared with the control and sham groups, mice treated with cystic fluid or ox-LDL gained weight during the 12-week period; however, this effect of ox-LDL was blocked by OXT pretreatment, and the body weight of mice pretreated with OXT was comparable with the weight of mice in the control and sham groups (Figure 4A and B), thus indicating that OXT could prevent ox-LDL-induced weight gain. Compared with the control and sham groups, immunostaining showed that the number of proopiomelanocortin (POMC) neurons in the ARC of mice treated with cystic fluid or ox-LDL was significantly reduced and that the fluorescence intensity of NPY was significantly increased, whereas OXT pretreatment blocked this effect (Figure 4C–E). The number of SMI32-immunoreactive axonal spheroids were steeply increased in the ME of mice treated with cystic fluid or ox-LDL, accompanied by the activation of microglia and the decreased fluorescence intensity of GnRH in the ARC; these effects of ox-LDL were blocked by OXT pretreatment (Figure 4F–J, Supplementary Figure 25K). Our results suggest that OXT pretreatment

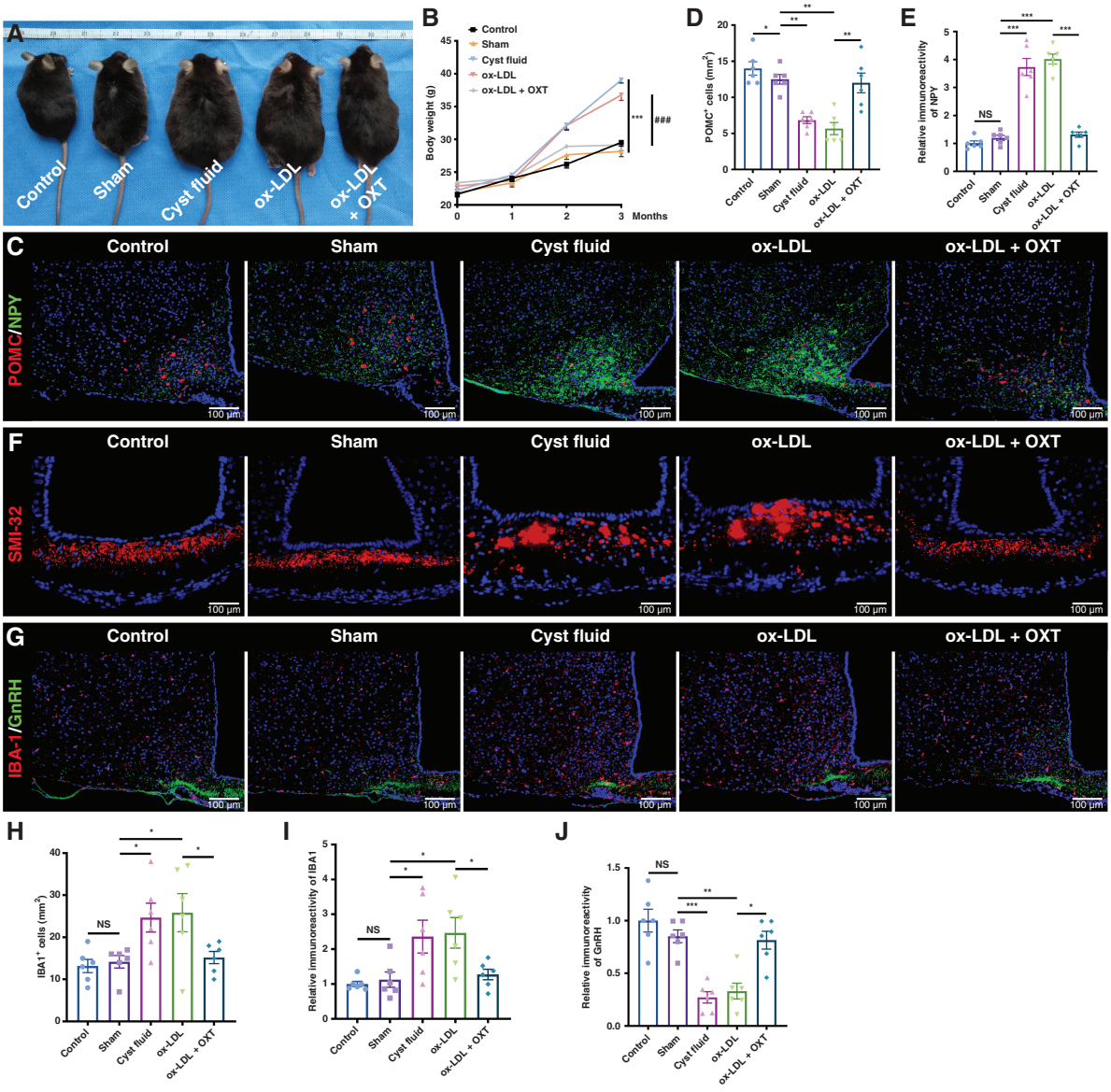

Figure 4. OXT blocks ox-LDL-induced hypothalamic dysfunction in mice. (A) Representative images of control mouse, sham surgery mouse, and mouse treated with cystic fluid, ox-LDL, and ox-LDL + OXT 3 months after the LV localization injection. (B) Body weight of the mice treated as described in (A) and measured at 0, 1, 2, and 3 months after the LV localization injection. (C) Double immunofluorescence staining of the ARC of mice treated with cystic fluid or ox-LDL ± OXT. Representative images of POMC and NPY staining. (D) Quantification of the POMC$^+$ cells described in (C) (n = 6/group). (E) Quantification of the NPY fluorescence intensity in the ARC of mice described in (C) (n = 6/group). (F) Immunofluorescence staining of the ME of mice treated with cystic fluid or ox-LDL ± OXT. Representative images of SMI-32 staining. (G) Double immunofluorescence staining of the ME of mice treated with cystic fluid or ox-LDL ± OXT. Representative images of IBA-1 and GnRH staining. (H) Quantification of the IBA-1$^+$ microglia described in (G) (n = 6/group). (I and J) Quantification of the fluorescence intensity of IBA-1 (I) and GnRH (J) in the ME of mice described in (G) (n = 6/group). Data are presented as the mean ± SEM. $^*P < .05$, $^{**}P < .01$, $^{***}P < .001$, $^{\#\#\#}P < .001$, NS, not significant. Statistical analysis: (B, D, E, and H–J) one-way ANOVA followed by Fisher's LSD post hoc multiple comparison test.

effectively prevented the ox-LDL-induced hypothalamic dysfunction in mice.

Finally, we used the Morris water maze test to examine the efficacy of OXT pretreatment on ox-LDL-induced cognitive impairment in mice. Compared with the control and sham groups, mice exposed to cystic fluid or ox-LDL exhibited significantly prolonged escape latencies to find the platform in the positioning navigation experiment and reduced the percentage of the total time in the target quadrant in the space exploration experiment, whereas OXT pretreatment blocked these effects (Supplementary Figure 25A–C). The hippocampus is closely associated with cognitive and memory functions. IBA-1$^+$ microglia and GFAP$^+$ astrocytes were abundant in the hippocampus

in the cystic fluid and ox-LDL group. OXT administration induced a dramatic decrease in microglia and astrocytes in the hippocampal region (Supplementary Figure 25D, G and H). However, compared with the control and sham groups, cystic fluid and ox-LDL did not significantly increase the senescence phenotype of NSCs in the hippocampus (Supplementary Figure 25E, F, I and J). Therefore, OXT can improve ox-LDL-induced memory and cognitive impairments by suppressing the inflammatory microenvironment in the hippocampus.

Discussion

The hypothalamus, including 3VF, is one of the smallest parts of the brain but is a critical structure that is responsible for establishing and maintaining homeostasis in systemic physiology.[19] Hypothalamic dysfunction and low long-term quality of life due to ACP have been a focus of research.[3,4] In the present study, nerve damage, which may be caused by multiple proinflammatory processes, was prevalent in 3VF adjacent to ACP. These pathological phenomena could explain the hypothalamic dysfunction and other associated complications that often occur in ACP patients. This finding was consistent with previous reports on the injection of ACP cystic fluid into rodent brain leading to proinflammatory response and neuronal damage and even causing obesity phenotype and growth retardation.[20–24]

htNSCs, a newly discovered type of NSCs in the hypothalamus, could delay and even reverse various aspects of aging throughout the body.[10,25] Similarly, tanycytes that line the 3VF also have the properties of NSCs and play an important role in the repair of nerve damage.[6] In the current study, a large number of htNSCs was recruited to the damaged 3VF adjacent to ACP, which could be derived from tanycytes. The multidirectional differentiation properties of NSCs, especially the ability to differentiate into functional neurons, may allow them to participate in the repair of nerve damage.[6,26] Owing to DNA damage and senescence, the recruited htNSCs could not participate in the repair of nerve damage. Moreover, htNSC senescence was mainly attributed to the activation of the P21 signaling pathway.

Lipid metabolism is critical for the regulation of NSCs.[8] Previous studies have also reported that lipid metabolism is involved in the regulation of mouse adult NSPC activity and adult neurogenesis in the hippocampus.[8] Furthermore, disrupted lipid metabolism triggers the accumulation of LDs inside NSCs, thus stressing NSCs and reducing their ability to divide[8]; this suggests that LDL-C may affect htNSC senescence. In the current study, we confirmed that lipids induced the aggregation of LDs in htNSCs, which led to DNA damage and htNSC senescence, and showed that the pretreatment of htNSCs with SSO protected htNSCs from ox-LDL-induced LD accumulation and lipotoxicity.

Protein quality control is essential for normal cell function; hence, the loss of protein homeostasis is associated with various age-related diseases.[12,13] In the current study, transcriptome sequencing analysis showed that ISR signaling was activated in htNSCs. Blocking lipid-induced ISR signaling activation inhibits inflammation and reduces atherosclerosis,[27] thus providing a potential mechanism of lipotoxicity in htNSCs. In the current study, the cystic fluid of ACP or ox-LDL induced ISR signaling activation in htNSCs in vitro. The pretreatment of htNSCs with ISRIB or GSK effectively prevented DNA damage and htNSC senescence despite ISRIB and GSK have no significant effect on LD accumulation. SSO blocks lipid entry, whereas the ISR signaling inhibitors decrease downstream signaling activation induced by lipids, thus blocking their negative effects on htNSC proliferation or neuronal differentiation.

The OXTR is widely distributed in the CNS and participates in the regulation of various functions.[28,29] Recently, several studies have reported that cognitive and memory functions, and hypothalamic obesity in ACP patients were significantly improved by intranasal OXT supplementation.[15,30] OXT not only suppresses SASP-induced senescence in NHDFs by OXTR-mediated extracellular signal–regulated kinase/Nrf2 signaling,[17] but also suppresses the inflammatory responses induced by LPS via the inhibition of the eIF-2α-ATF4 pathway in mouse microglia.[18] In the current study, the axons of OXT-transporting neurons in the 3VF adjacent to ACP were significantly damaged. OXT pretreatment effectively blocked ox-LDL-induced DNA damage and htNSC senescence. Similar to ISR signaling inhibitors, OXT had no significant effect on LD accumulation in htNSCs but showed a function similar to ISR signaling inhibitors and prevented lipotoxicity in htNSCs by blocking ISR signaling, thereby improving hypothalamic dysfunction. Furthermore, the inflammatory microenvironment caused by ox-LDL in hippocampus was also avoided by OXT and accompanied by the improvement of cognitive function.

The BBB in 3VF adjacent to ACP was disrupted, thus resulting in peripheral mononuclear macrophage and lymphocyte infiltration. The infiltration of peripheral immune cells into the brain is often accompanied with a series of proinflammatory responses, thus leading to neurological disorders, including obesity, cognitive and memory disorders, and anxiety.[31–33] By using mouse models, we demonstrated that OXT pretreatment prevented ox-LDL-induced BBB damage and peripheral immune cell infiltration. This protective effect of OXT on the BBB was observed not only in vascular endothelium but also in the ependymal layer; however, the exact protective mechanism of OXT on the BBB remains unclear. In ACP patients, the BBB is often significantly damaged prior to surgical intervention and is further aggravated after surgery. Therefore, in ACP patients with hypothalamic obesity, the high concentration of LDL-C in the blood may aggravate lipotoxicity in htNSCs and trigger peripheral immune cell infiltration via the damaged BBB, thus forming a vicious cycle.

ACP was capable of high synthesis and high efflux lipids; this finding is consistent with those of previous studies.[7,21,34] LXRα, a key protein of cholesterol transport, was closely associated with the activation of the WNT signaling pathway in the 3VF adjacent to ACP and the cystic wall[35,36]; this explained the accumulation of lipids secreted by ACP in the 3VF adjacent to ACP and the cyst lumen. The nuclear translocation of β-catenin in the epithelial whorls of ACP is accompanied by senescence and high efflux of

lipids. Whether there is a relationship between them remains unclear. The senescence phenotype of β-catenin-accumulating clusters could promote the proliferation of ACP cells[7,37,38]; therefore, whether the senescent htNSCs in the adjacent 3VF has the same effect is an interesting future research topic.

OXT treatment in ACP patients could repair the integrity of BBB and reduce the inflammatory response activated by the infiltrated peripheral immune cells, thus blocking the lipotoxicity of htNSCs induced by the diffusion of peripheral LDL-C into the 3VF. Meanwhile, OXT prevents the continuous occurrence of lipotoxic events of htNSCs by blocking ISR signaling. However, this study is limited by the difficulty in modeling, including the injection of cystic fluid or intracranial xenograft of ACP cells into the mouse ME. Moreover, given that normal human htNSCs could not be obtained, we used NSCs from relatively normal SVZ far away from the frontal glioma, which cannot be considered strict controls. We also validated the findings via various experimental methods and received similar results under the current experimental conditions.

In conclusion, reducing LD aggregation or blocking ISR signaling in htNSCs may effectively prevent htNSC senescence and could be used as a potential therapeutic target to improve hypothalamic function and the long-term quality of life of ACP patients.

Supplementary material

Supplementary material is available online at *Neuro-Oncology* (http://neuro-oncology.oxfordjournals.org/).

Keywords

ACP | htNSCs | ISR signaling | lipid-induced senescence | oxytocin

Acknowledgements

The authors would like to thank Binghui Qiu for excellent technical support and patient care.

Funding

This study was supported by grants from the National Natural Science Foundation of China (grant nos. 82103033, 82002646, and 81972352).

Conflict of interest: The authors declare that they have no potential conflicts of interest.

Authorship Statement

C.H.W., H.R.Z., Q.L., and R.R.G. designed and conducted in vivo and in vitro experiments, performed data analysis, and wrote the manuscript. Q.C.Z., Y.W.F., and C.D.W. performed the in vitro experiments. J.S. and P.L. conducted in vivo experiments. J.P., J.X.P., J.F., and Y.L. provided clinical specimens. Y.W.L., X.Y.Q., and Y.Y.D. analyzed the data. C.H.W., H.R.Z., J.F., Q.L., and R.R.G. contributed equally to this work. Y.L. and S.T.Q. designed the experiment, interpreted the data, wrote the manuscript, and approved the final version of the manuscript for publication. All authors read and helped to edit the final manuscript.

References

1. Olsson DS, Andersson E, Bryngelsson IL, Nilsson AG, Johannsson G. Excess mortality and morbidity in patients with craniopharyngioma, especially in patients with childhood onset: a population-based study in Sweden. *J Clin Endocrinol Metab.* 2015;100(2):467–474.
2. Müller HL, Merchant TE, Warmuth-Metz M, Martinez-Barbera JP, Puget S. Craniopharyngioma. *Nat Rev Dis Primers.* 2019;5(1):75.
3. Sterkenburg AS, Hoffmann A, Gebhardt U, et al. Survival, hypothalamic obesity, and neuropsychological/psychosocial status after childhood-onset craniopharyngioma: newly reported long-term outcomes. *Neuro Oncol.* 2015;17(7):1029–1038.
4. Poretti A, Grotzer MA, Ribi K, Schönle E, Boltshauser E. Outcome of craniopharyngioma in children: long-term complications and quality of life. *Dev Med Child Neurol.* 2004;46(4):220–229.
5. Scheltens P, De Strooper B, Kivipelto M, et al. Alzheimer's disease. *Lancet.* 2021;397(10284):1577–1590.
6. Mu W, Li S, Xu J, et al. Hypothalamic Rax(+) tanycytes contribute to tissue repair and tumorigenesis upon oncogene activation in mice. *Nat Commun.* 2021;12(1):2288.
7. Apps JR, Carreno G, Gonzalez-Meljem JM, et al. Tumour compartment transcriptomics demonstrates the activation of inflammatory and odontogenic programmes in human adamantinomatous craniopharyngioma and identifies the MAPK/ERK pathway as a novel therapeutic target. *Acta Neuropathol.* 2018;135(5):757–777.
8. Bowers M, Liang T, Gonzalez-Bohorquez D, et al. FASN-dependent lipid metabolism links neurogenic stem/progenitor cell activity to learning and memory deficits. *Cell Stem Cell.* 2020;27(1):98–109.e11.
9. Zhang G, Li J, Purkayastha S, et al. Hypothalamic programming of systemic ageing involving IKK-β, NF-κB and GnRH. *Nature.* 2013;497(7448):211–216.
10. Xiao YZ, Yang M, Xiao Y, et al. Reducing hypothalamic stem cell senescence protects against aging-associated physiological decline. *Cell Metab.* 2020;31(3):534–548.e5.
11. Khatana C, Saini NK, Chakrabarti S, et al. Mechanistic insights into the oxidized low-density lipoprotein-induced atherosclerosis. *Oxid Med Cell Longev.* 2020;2020:5245308. https://www.hindawi.com/journals/omcl/2020/5245308/
12. Costa-Mattioli M, Gobert D, Harding H, et al. Translational control of hippocampal synaptic plasticity and memory by the eIF2alpha kinase GCN2. *Nature.* 2005;436(7054):1166–1173.
13. Costa-Mattioli M, Gobert D, Stern E, et al. eIF2alpha phosphorylation bidirectionally regulates the switch from short- to long-term synaptic plasticity and memory. *Cell.* 2007;129(1):195–206.

14. Harding HP, Zhang Y, Zeng H, et al. An integrated stress response regulates amino acid metabolism and resistance to oxidative stress. *Mol Cell.* 2003;11(3):619–633.
15. Gebert D, Auer MK, Stieg MR, et al. De-masking oxytocin-deficiency in craniopharyngioma and assessing its link with affective function. *Psychoneuroendocrinology.* 2018;88:61–69. https://www.sciencedirect.com/science/article/abs/pii/S030645301731257X?via%3Dihub
16. Hsu EA, Miller JL, Perez FA, Roth CL. Oxytocin and naltrexone successfully treat hypothalamic obesity in a boy post-craniopharyngioma resection. *J Clin Endocrinol Metab.* 2018;103(2):370–375.
17. Cho SY, Kim AY, Kim J, et al. Oxytocin alleviates cellular senescence through oxytocin receptor-mediated extracellular signal-regulated kinase/Nrf2 signalling. *Br J Dermatol.* 2019;181(6):1216–1225.
18. Inoue T, Yamakage H, Tanaka M, et al. Oxytocin suppresses inflammatory responses induced by lipopolysaccharide through inhibition of the eIF-2-ATF4 pathway in mouse microglia. *Cells.* 2019;8(6):527.
19. Cakir I, Nillni EA. endoplasmic reticulum stress, the hypothalamus, and energy balance. *Trends Endocrinol Metab.* 2019;30(3):163–176.
20. Tena-Suck ML, Hernández-Campos ME, Ortiz-Plata A, et al. Intracerebral injection of oil cyst content of human craniopharyngioma (oil machinery fluid) as a toxic model in the rat brain. *Acta Histochem.* 2014;116(3):448–456.
21. Tena-Suck ML, Morales-Del Ángel AY, Hernández-Campos ME, et al. Ultrastructural characterization of craniopharyngioma at the tumor boundary: a structural comparison with an experimental toxic model using "oil machinery" fluid, with emphasis on Rosenthal fibers. *Acta Histochem.* 2015;117(8):696–704.
22. Ghosh M, Das S, Rao K, et al. Effects of craniopharyngioma cyst fluid on neurons and glial cells cultured from rat brain hypothalamus. *J Chem Neuroanat.* 2018;94:93–101. https://pubmed.ncbi.nlm.nih.gov/30339791/
23. Donson AM, Apps J, Griesinger AM, et al. Molecular analyses reveal inflammatory mediators in the solid component and cyst fluid of human adamantinomatous craniopharyngioma. *J Neuropathol Exp Neurol.* 2017;76(9):779–788.
24. Ainiwan Y, Chen Y, Mao C, et al. Adamantinomatous craniopharyngioma cyst fluid can trigger inflammatory activation of microglia to damage the hypothalamic neurons by inducing the production of β-amyloid. *J Neuroinflammation.* 2022;19(1):108.
25. Zhang Y, Kim MS, Jia B, et al. Hypothalamic stem cells control ageing speed partly through exosomal miRNAs. *Nature.* 2017;548(7665):52–57.
26. Zahr SK, Kaplan DR, Miller FD. Translating neural stem cells to neurons in the mammalian brain. *Cell Death Differ.* 2019;26(12):2495–2512.
27. Onat UI, Yildirim AD, Tufanli O, et al. Intercepting the lipid-induced integrated stress response reduces atherosclerosis. *J Am Coll Cardiol.* 2019;73(10):1149–1169.
28. Jurek B, Neumann ID. The oxytocin receptor: from intracellular signaling to behavior. *Physiol Rev.* 2018;98(3):1805–1908.
29. Neumann ID, Slattery DA. Oxytocin in general anxiety and social fear: a translational approach. *Biol Psychiatry.* 2016;79(3):213–221.
30. Brandi ML, Gebert D, Kopczak A, Auer MK, Schilbach L. Oxytocin release deficit and social cognition in craniopharyngioma patients. *J Neuroendocrinol.* 2020;32(5):e12842.
31. Valdearcos M, Douglass JD, Robblee MM, et al. Microglial inflammatory signaling orchestrates the hypothalamic immune response to dietary excess and mediates obesity susceptibility. *Cell Metab.* 2017;26(1):185–197.e3.
32. Yao J, Wu D, Zhang C, et al. Macrophage IRX3 promotes diet-induced obesity and metabolic inflammation. *Nat Immunol.* 2021;22(10):1268–1279.
33. Wohleb ES, McKim DB, Shea DT, et al. Re-establishment of anxiety in stress-sensitized mice is caused by monocyte trafficking from the spleen to the brain. *Biol Psychiatry.* 2014;75(12):970–981.
34. Wang CH, Qi ST, Fan J, et al. Identification of tumor stem-like cells in admanatimomatous craniopharyngioma and determination of these cells' pathological significance. *J Neurosurg.* 2019;133(3):664–674.
35. Andoniadou CL, Gaston-Massuet C, Reddy R, et al. Identification of novel pathways involved in the pathogenesis of human adamantinomatous craniopharyngioma. *Acta Neuropathol.* 2012;124(2):259–271.
36. Hölsken A, Buchfelder M, Fahlbusch R, Blümcke I, Buslei R. Tumour cell migration in adamantinomatous craniopharyngiomas is promoted by activated Wnt-signalling. *Acta Neuropathol.* 2010;119(5):631–639.
37. Gonzalez-Meljem JM, Haston S, Carreno G, et al. Stem cell senescence drives age-attenuated induction of pituitary tumours in mouse models of paediatric craniopharyngioma. *Nat Commun.* 2017;8(1):1819.
38. Gonzalez-Meljem JM, Martinez-Barbera JP. Adamantinomatous craniopharyngioma as a model to understand paracrine and senescence-induced tumourigenesis. *Cell Mol Life Sci.* 2021;78(10):4521–4544.